State feedback control of advanced static var compensator using a five-level NPC inverter topology

Mansour Benyamina[1], Ali Tahri[2], Abdelkader Boukortt[3]

[1,3]Department of Electrical Engineering, Abdelhamid Ibn Badis University of Mostaganem, Mostaganem, Algeria
[2]Department of Electrotechnics, University of Sciences and Technology of Oran USTO-MB, Bir El Djir, Algeria

Article Info	ABSTRACT
	This paper deals with the modeling and control of an advanced static var compensator (ASVC) using a five-level neutral point-clamped (NPC) voltage source inverter (VSI). The nonlinear state space model of the five-level ASVC is obtained from the d-q axis frame. The effectiveness of this compensator highly depends on the choice of the control strategy. The proposed state feedback control (SFC) technique is applied to adjust the ASVC Var flow with the AC transmission network and achieve DC voltage capacitor balance. The dynamic performance of the ASVC based SFC controller is evaluated under several operating conditions. The simulation results demonstrate that the proposed SFC control strategy is highly robust compared to the conventional Proportional-Integral (PI) control.

Corresponding Author:

Mansour Benyamina
Department of Electrical Engineering
FST Faculty, Abdelhamid Ibn Badis University
Site 1, Route Belahcel 27000, Mostaganem, Algeria
Email: mansour_benyamina@yahoo.fr

1. INTRODUCTION

The static compensators (STATCOM)s are important reactive compensation devices that have been used in power systems to maintain bus voltage at a constant level, improve the transient stability, damp the systems and suppress voltage flicker [1]-[4].

The introduction of modern semiconductor devices in the design of power electronic converters has resulted in a solid-state Var source with a simpler structure, namely the ASVC [5]-[7]. An ASVC is a fully controlled switch based converter, which is an upgrade version of The Static Var Compensators (SVCs), a thyristor-based converter. Like an SVC, the ASVC provides a controllable parallel compensation. The reactive power generation or absorption by an ASVC is the same as that of an SVC. The ASVC has advantages over a conventional SVC [8]-[11].

The ASVC use a Pulse Width Modulation (PWM) controlled DC-AC VSI with a capacitor as a DC power storage device. Recently, the multilevel PWM converter topology has drawn tremendous interest in the power industry since it can easily provide the high power required for high power applications for such uses as static VAR compensation, active power filters, and the control of large motors by high power adjustable frequency drives. The most popular structure proposed as a transformerless voltage source inverter is the diode clamped converter based on the neutral point clamped (NPC) converter proposed by Nabae [12], [13]. It has the advantages that the blocking voltage of each switching device is one half of DC-link voltage, and the harmonics contents output voltages are lower than those of a two-level inverter for the same switching frequency. The NPC inverter has the drawback of the unbalance DC capacitors voltage when used

as a static var compensator. Different methods were proposed to solve this issue. Some researchers have proposed to insert two inductors in one leg to balance the capacitors voltage [14], [15]. Others have introduced a modified switching pattern and improved the optimized PWM technique [16], [17].

This paper presents a modeling and analysis of this new type of five-level inverter used for static VAR compensation. The control design is based on the conventional proportional-integral (PI) controller and the state feedback controller (SFC) controllers to adjust the ASVC Var flow with the AC system. The SFC controller also has the ability to balance the total DC capacitors voltage without any extra device or design of a complex circuit or optimizing control method. Finally, some simulation results under various transient conditions of the proposed ASVC model and its control are given to prove their effectiveness.

2. OVERVIEW AND MODELING OF THE ASVC-BASED FIVE-LEVEL INVERTER

The ASVC circuit consists of twenty four-pulse VSI with four DC capacitors and a PWM modulator. The ASVC is connected to the transmission line is via a coupling transformer where Rs and Ls are the coupling transformer active losses and leakage respectively, as shown in Figure 1 [18]-[22].
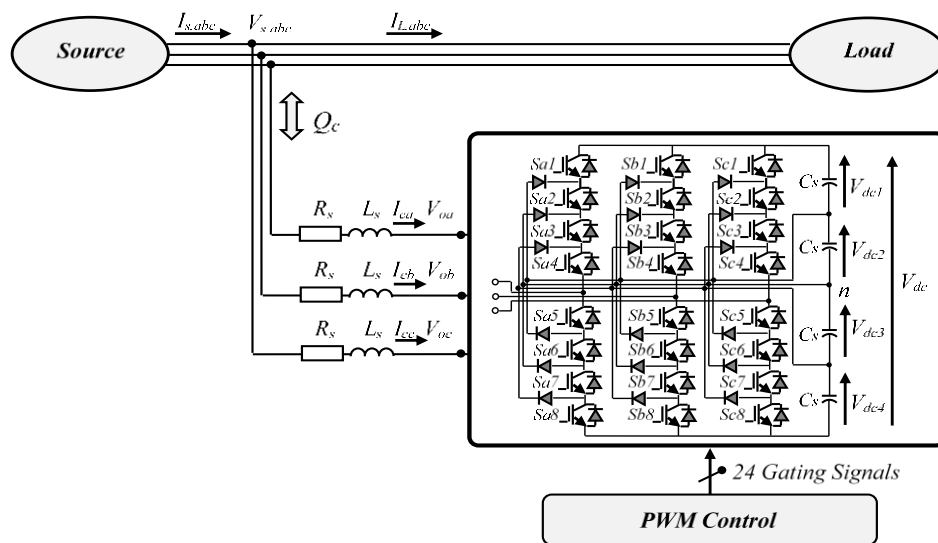

Figure 1. Power circuit of the ASVC-based five-level NPC-VSI inverter

where,

$I_{s,abc}$, $I_{L,abc}$: Supply and load currents. $I_{c,abc}$: ASVC currents.
$V_{s,abc}$: Supply voltages. $V_{o,abc}$: Inverter output voltage.
$V_{dc,i}$: Capacitor voltages at different levels. V_{dc} : Total DC side voltage of the Inverter.
$I_{dc,i}$: DC side current. C_s : DC side capacitor.

2.1. PWM control strategy of the five-level NPC-VSI inverter

In this work, the PWM control strategy for a five-level inverter uses a single reference and four carriers signals as depicted in Figure 2(a) where a sinusoidal reference signal is continuously compared to four (N-1 in general) triangle waveforms where N is the number of level of the inverter. One of advantages of this technique is that the significant harmonics are concentrated at the carrier frequency [23]-[26].

The frequency modulation index and the amplitude modulation index are given by (1)

$$\begin{cases} m_f = \dfrac{f_c}{f_s} \\ m_a = \dfrac{2\,A_s}{A_c\,(N-1)} \end{cases} \tag{1}$$

where
f_c : Frequency of carries. A_c : Peak-to-peak amplitude of carries.

f_s : Frequency of reference. A_s : Peak amplitude of reference.

The mathematical model of the converter is developed using switch connection function F_{ki} , $(k=a,b,c)$: names of arms and $(i=0,1,2,3,4)$: number of the function. The switching function, is either 1 or 0 corresponding to on and off states of switch S_{ki} , $(k=a,b,c)$: names of arms and $(i=1,2,3,4,5,6,7,8)$: number of the switches of one arm. Table 1 lists the switch connection function of one leg and output voltage.

Table 1. A possible switch combination of one phase leg for the NPC-based five-level inverter

F_{ki}	S_{a1}	S_{a2}	S_{a3}	S_{a4}	S_{a5}	S_{a6}	S_{a7}	S_{a8}	V_{oa}
F_{a1}	1	1	1	1	0	0	0	0	$V_{dc}/2$
F_{a2}	0	1	1	1	1	0	0	0	$V_{dc}/4$
F_{a0}	0	0	1	1	1	1	0	0	0
F_{a3}	0	0	0	1	1	1	1	0	$-V_{dc}/4$
F_{a4}	0	0	0	0	1	1	1	1	$-V_{dc}/2$

Using the upper arm of the phase-leg 'a' as an example shown by Figure 2(b). Note that the switch states S_{a1}, S_{a2}, S_{a3} and S_{a4} are complementary to S_{a5}, S_{a6}, S_{a7} and S_{a8} respectively [27], [28].
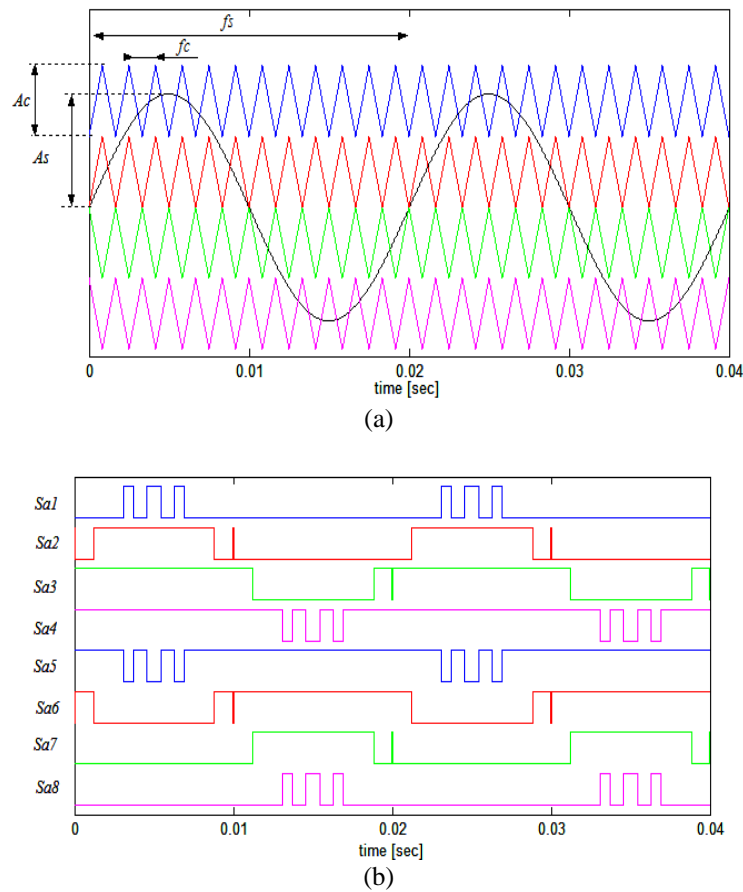

(a)

(b)

Figure 2. (a) Five-level PWM control ($m_f=12$ and $m_a=0.8$), (b) States of switch

2.2. Mathematical model of the ASVC system

The simplified three-phase equivalent circuit of the ASVC connected to a transmission line is shown in Figure 3. The ASVC supplies reactive power to the AC transmission system if the magnitude of the output inverter voltage is greater than the AC terminal voltage and absorb reactive power from the AC transmission system if the magnitude of the AC terminal voltage is greater than the output inverter voltage. The Var exchange is zero when the two voltages are equal [29], [30].
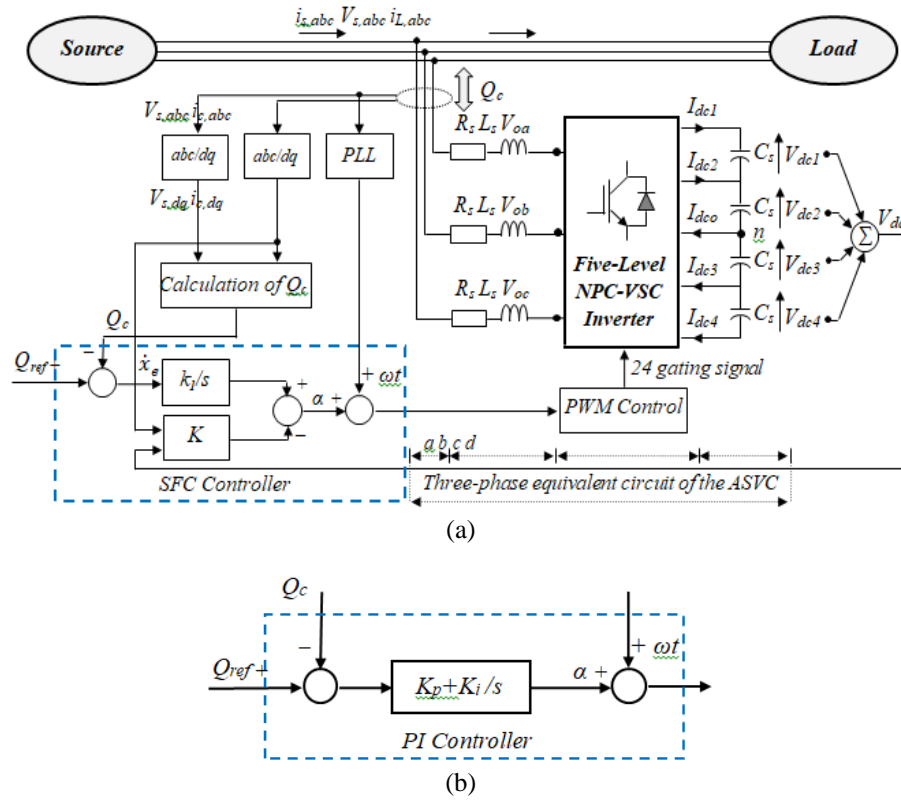
(a)

(b)

Figure 3. ASVC closed-loop control system, (a) With SFC controller, (b) With PI controller

a : Three-phase source voltage, b : Coupling transformer.
c : PWM voltage source inverter, d : DC side capacitors.

It is assumed that the AC side is a balanced sinusoidal three-phase voltage supply. Using matrix form, the mathematical model of the ASVC system is given by (2):

$$\frac{d}{dt}\begin{bmatrix} i_{ca} \\ i_{cb} \\ i_{cc} \end{bmatrix} = \begin{bmatrix} -\frac{R_S}{L_S} & 0 & 0 \\ 0 & -\frac{R_S}{L_S} & 0 \\ 0 & 0 & -\frac{R_S}{L_S} \end{bmatrix}\begin{bmatrix} i_{ca} \\ i_{cb} \\ i_{cc} \end{bmatrix} + \frac{1}{L_S}\begin{bmatrix} V_{sa} - V_{oa} \\ V_{sb} - V_{ob} \\ V_{sc} - V_{oc} \end{bmatrix} \tag{2}$$

The output inverter voltages relative to the point n and the DC side currents of the inverter using the connection functions are given in (3)-(7):

$$\begin{bmatrix} V_{oa} \\ V_{ob} \\ V_{oc} \end{bmatrix} = \frac{1}{3}\begin{bmatrix} 2 & -1 & -1 \\ -1 & 2 & -1 \\ -1 & -1 & 2 \end{bmatrix}(F_A.V_{dc1} + F_B.V_{dc2} - F_C.V_{dc3} - F_D.V_{dc4}) \tag{3}$$

$$\begin{bmatrix} I_{dc1} \\ I_{dc2} \\ I_{dc3} \\ I_{dc4} \end{bmatrix} = \begin{bmatrix} F_{a1} & F_{b1} & F_{c1} \\ F_{a2} & F_{b2} & F_{c2} \\ F_{a3} & F_{b3} & F_{c3} \\ F_{a4} & F_{b4} & F_{c4} \end{bmatrix}\begin{bmatrix} i_{ca} \\ i_{cb} \\ i_{cc} \end{bmatrix} \tag{4}$$

$$I_{dco} = I_{dc1} + I_{dc2} - I_{dc3} - I_{dc4} \tag{5}$$

with:

$$\begin{cases} F_A = [F_{a1} \quad F_{b1} \quad F_{c1}]^T \\ F_B = [F_{a2} \quad F_{b2} \quad F_{c2}]^T \\ F_C = [F_{a3} \quad F_{b3} \quad F_{c3}]^T \\ F_D = [F_{a4} \quad F_{b4} \quad F_{c4}]^T \end{cases} \tag{6}$$

$$\begin{cases} V_{dc1} = V_{dc}/2 \\ V_{dc2} = V_{dc}/4 \\ V_{dc3} = -V_{dc}/4 \\ V_{dc4} = -V_{dc}/2 \end{cases} \tag{7}$$

The model of the DC side capacitors voltages is given by (8):

$$\frac{d}{dt}\begin{bmatrix} V_{dc1} \\ V_{dc2} \\ V_{dc3} \\ V_{dc4} \end{bmatrix} = \frac{1}{C_s}\begin{bmatrix} I_{dc1} \\ I_{dc2} \\ I_{dc3} \\ I_{dc4} \end{bmatrix} \tag{8}$$

Therefore, by using the *d-q* frame transform, the nonlinear state-space model of the ASVC based on the five-level inverter combined the DC circuit equation can be expressed by (9):

$$\frac{d}{dt}\begin{bmatrix} i_q \\ i_d \\ V_{dc} \end{bmatrix} = \begin{bmatrix} -\frac{R_s}{L_s} & -\omega & 0 \\ -\omega & -\frac{R_s}{L_s} & -\frac{m}{L_s} \\ 0 & -\frac{m}{4C_s} & 0 \end{bmatrix}\begin{bmatrix} i_q \\ i_d \\ V_{dc} \end{bmatrix} + \frac{V_s}{L_s}\begin{bmatrix} \sin\alpha \\ \cos\alpha \\ 0 \end{bmatrix} \tag{9}$$

where *m* is the ratio relating the AC to the DC voltage.

The modulation index relates the maximum phase voltage $V_{o,Peak}$ to the total DC side voltage V_{dc} is given by (10):

$$MI = \sqrt{\frac{2}{3}}\, m = \frac{V_{o,Peak}}{V_{dc}} \tag{10}$$

The obtained state equation is non-linear, with respect to the control variable α which is related to the phase difference between the source voltage and inverter output voltage. In the range of small values of α ($|\alpha| < 5°$), the small-signal equivalent state equations and the reactive power delivered by the ASVC-based five-level inverter system in the *d-q* frame is expressed as (11) and (12) [18]:

$$\frac{d}{dt}\begin{bmatrix} \Delta i_q \\ \Delta i_d \\ \Delta V_{dc} \end{bmatrix} = \begin{bmatrix} -\frac{R_s}{L_s} & -\omega & 0 \\ -\omega & -\frac{R_s}{L_s} & -\frac{m}{L_s} \\ 0 & -\frac{m}{4C_s} & 0 \end{bmatrix}\begin{bmatrix} \Delta i_q \\ \Delta i_d \\ \Delta V_{dc} \end{bmatrix} + \frac{V_s}{L_s}\begin{bmatrix} -1 \\ 0 \\ 0 \end{bmatrix}\Delta\alpha \tag{11}$$

$$\Delta Q_c = [-V_s \quad 0 \quad 0][\Delta i_q \quad \Delta i_d \quad \Delta V_{dc}]^T \tag{12}$$

from (11) and (12), the transfer function of the ASVC-based five-level inverter system is given by:

$$G_p(s) = \frac{\Delta Q_c(s)}{\Delta\alpha(s)} = C(sI - A)^{-1}B = \frac{N(s)}{D(s)} \tag{13}$$

with

$$N(s) = V_s^2\left(\frac{s^2}{L_s} + \frac{R_s}{L_s}s + \frac{m^2}{4\,L_s^2\,C_s}s\right) \tag{14}$$

$$D(s) = s^3 + 2\frac{R_s}{L_s}s^2 + \left(\omega^2 + \frac{R_s^2}{L_s^2} + \frac{m^2}{4\,L_s\,C_s}\right)s + \frac{m^2 R_s}{4\,L_s^2\,C_s} \tag{15}$$

3. CONTROL SCHEME OF THE ASVC SYSTEM

3.1. PI controller design

Figure 4 shows the block diagram of the ASVC-based five-level inverter system controlled by PI controller. The transfer function of the controller is expressed as (16):

$$G_c(s) = K_p + \frac{K_i}{s} \tag{16}$$

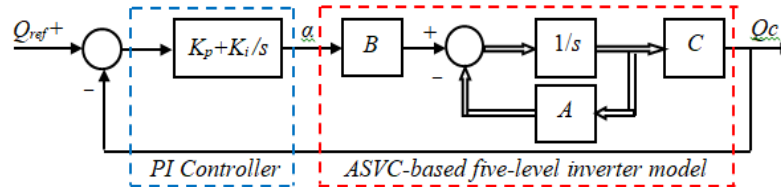The PI parameters are calculated using root locus design for a damping factor 0.7.

Figure 4. Block diagram of the ASVC system with PI control

3.2. The State feedback controller

The overall closed loop control of the ASVC-based five-level inverter with SFC control technique is shown in Figure 3(a) and the cascade control system of the state-feedback configuration is given in Figure 5 [31], [32]. The controlled variable Q_c is compared with the set-point value Q_{ref} and the control error is fed back to an integrator. The former feed forward gain k_1 is now the gain of the integrator. This configuration shows that the gain K in the internal closed-loop is a feedback parameter.

The basic principle of the designed system is to insert an integrator in the feed forward path between the error comparator and the process [31].
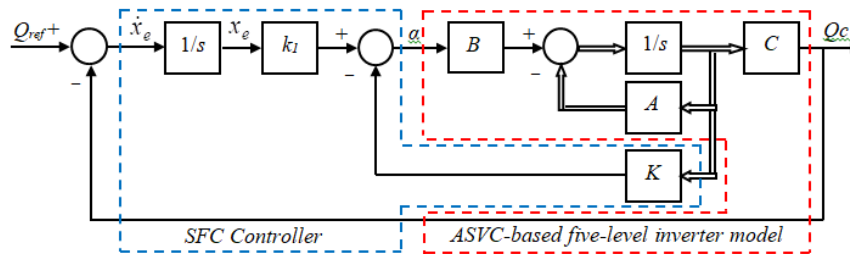

Figure 5. Block diagram of the ASVC system with SFC control

From the block diagram of Figure 5 we get:

$$\begin{cases} \dot{x} = Ax + Bu \\ \quad Q_c = Cx \end{cases} \tag{17}$$

$$u = -Kx + k_1 x_e \tag{18}$$

$$\dot{x}_e = Q_{ref} - Q_c = Q_{ref} - Cx \tag{19}$$

We assume that the state equation given by (17) is completely state controllable. The augmented dynamic system can be described by an equation that is combination of (17) and (19).

$$\begin{bmatrix} \dot{x}(t) \\ \dot{x}_e(t) \end{bmatrix} = \begin{bmatrix} A & 0 \\ -C & 0 \end{bmatrix} \begin{bmatrix} x(t) \\ x_e(t) \end{bmatrix} + \begin{bmatrix} B \\ 0 \end{bmatrix} u(t) + \begin{bmatrix} 0 \\ 1 \end{bmatrix} Q_{ref}(t) \tag{20}$$

$$Q_c = [C \quad 0]\begin{bmatrix} x(t) \\ x_e(t) \end{bmatrix} \tag{21}$$

$$u = [-K \quad k_1]\begin{bmatrix} x(t) \\ x_e(t) \end{bmatrix} \tag{22}$$

where:

$$\hat{A} = \begin{bmatrix} A & 0 \\ -C & 0 \end{bmatrix}; \ \hat{B} = \begin{bmatrix} B \\ 0 \end{bmatrix}; \ \hat{C} = [C \quad 0] \tag{23}$$

We shall design an asymptotically stable system such that x(∞), xe(∞), and u(∞) approach constant values, respectively. Then, at steady state $\dot{x}_e(\infty) = 0$, we get $Q_c(\infty) = Q_{ref}$.

The aim of the proposed SFC controller is to regulate the total DC side voltage V_{dc} which is the sum of the four capacitors voltages on the DC side of the inverter, the AC-current components I_{dq} and the reactive power response Q_c.

The state space representation of the ASVC based upon five-level inverter controlled by SFC-controller can be described by an equation that is combination of (11) and (12).

$$\frac{d}{dt}\begin{bmatrix} \Delta i_q \\ \Delta i_d \\ \Delta V_{dc} \\ \Delta x_e \end{bmatrix} = \begin{bmatrix} -\frac{R_s}{L_s} & -\omega & 0 & 0 \\ -\omega & -\frac{R_s}{L_s} & -\frac{m}{L_s} & 0 \\ 0 & -\frac{m}{4C_s} & 0 & 0 \\ V_s & 0 & 0 & 0 \end{bmatrix}\begin{bmatrix} \Delta i_q \\ \Delta i_d \\ \Delta V_{dc} \\ \Delta x_e \end{bmatrix} + \begin{bmatrix} -\frac{V_s}{L_s} \\ 0 \\ 0 \\ 0 \end{bmatrix}\Delta\alpha \tag{24}$$

$$\Delta Q_c = [-V_s \quad 0 \quad 0 \ 0][\Delta i_q \quad \Delta i_d \quad \Delta V_{dc} \ \Delta x_e]^T \tag{25}$$

To achieve a good dynamic response of the closed loop system, the poles are determined by the Ackermann algorithm where:

$$p_1 = -500, p_2 = -450, p_3 = -300 + 305.65i, p_4 = -300 - 305.65i$$

The necessary state feedback gain matrix $\hat{K}$ are determined using the pole placement technique, where

$$\hat{K} = [K \vdots k_1] = [-0.0320 \ -0.0174 \ -0.0023 \ -0.0382]$$

4. SIMULATION RESULTS AND DISCUSSION

A digital simulation is done based on the detailed ASVC system shown by Figure 3. The PI and the SFC controllers' parameters are listed in Appendix.

The PI and SFC controllers were evaluated under more realistic simulation condition when the ASVC was controlled by PWM control circuit.

Figure 6 displays the simulation run for a step change in the Q_{ref} reference from 10 Kvar (inductive) to -10 Kvar (capacitive) in order to swing the system from leading to lagging mode at time 0.1 sec and standby mode at 0.2 sec.

From Figure 6, a performance comparison between the two controllers is summarized in Table 2. The SFC controller has a rise time and settling time of 12.4 msec and 30 msec respectively, where the PI controller has a rise time and settling time of 14.2 msec and 45.65 msec respectively. It can be seen that the rise time and the settling time of the SFC controller are 12.7 % and 35.5 % respectively less than those of the PI controller. Moreover, the SFC controller does not have any overshoot when the PI controller in transient state exhibits 5% of overshoot.

Table 2. The performance comparison between conventional PI and SFC controllers

Parameters	PI controller	SFC controller
Rise Time *(msec)*	14.20	12.40
Settling Time *(msec)*	45.65	30.00
Overshoot *(%)*	5	0

Figure 7 shows a phase current waveforms dynamic behavior. It is observed that the current injected into the transmission line controlled by the SFC controller is faster that the one controlled by PI. Figure 8 (a) and (b) show the source phase voltage and the inverter current waveforms respectively with PI and SFC controllers. At first, the ASVC is generating 10 kVar inductive reactive power and at 0.1 sec is fastly absorbing also 10 kVar but as a capacitive reactive power. From 0.2 sec the ASVC is in standby mode, it provides no reactive power (Qc=0 kVar). Figure 9 and Figure 10 represent transient DC side voltage across the four capacitors after a sudden change in reference under PI and SFC controllers respectively, it can be noticed that voltage fluctuation of $V_{dc1,2,3,4}$ with SFC controller were reduced by 50 % compared to those obtained with PI controller.

Figure 11(a)(b) and Figure 12(a)(b) show the transient response of the total DC side voltage V_{dc}, and I_d, I_q AC-current components respectively with PI and SFC controllers. It can be seen that total side voltage controlled by the SFC is better that the one controlled by PI.

The source voltage and inverter output voltage waveforms of the five-level NPC inverter for reactive power compensation with PI and SFC controllers are depicted by Figure 13 (a) and (b) respectively.
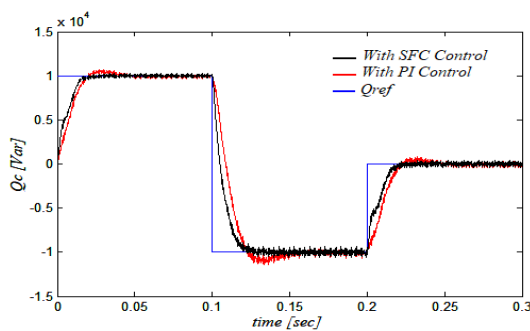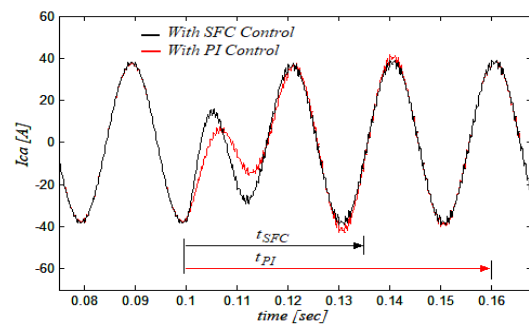

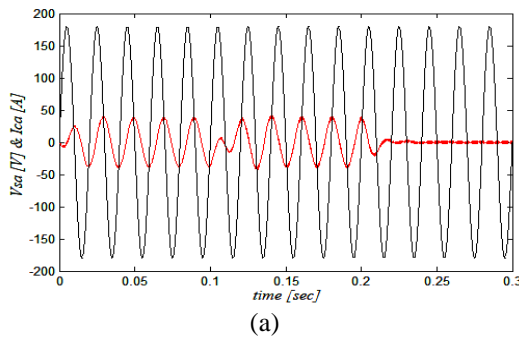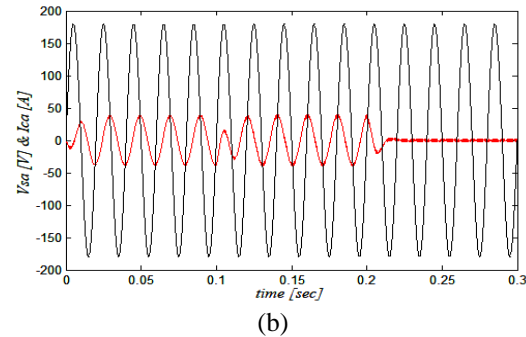Figure 6. Reactive power response
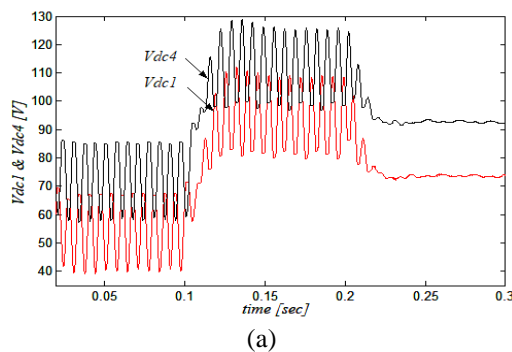

Figure 7. a-phase AC current response
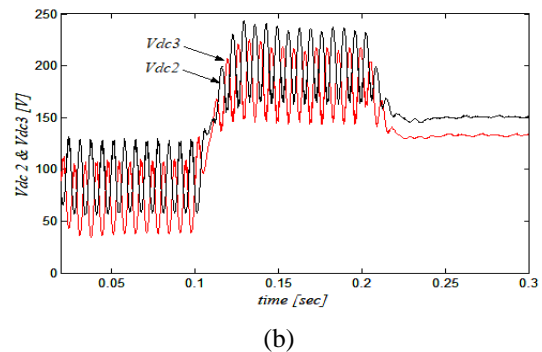

(a)

(b)

Figure 8. Source voltage and AC current Waveforms. (a) with PI control, (b) with SFC control

(a)

(b)

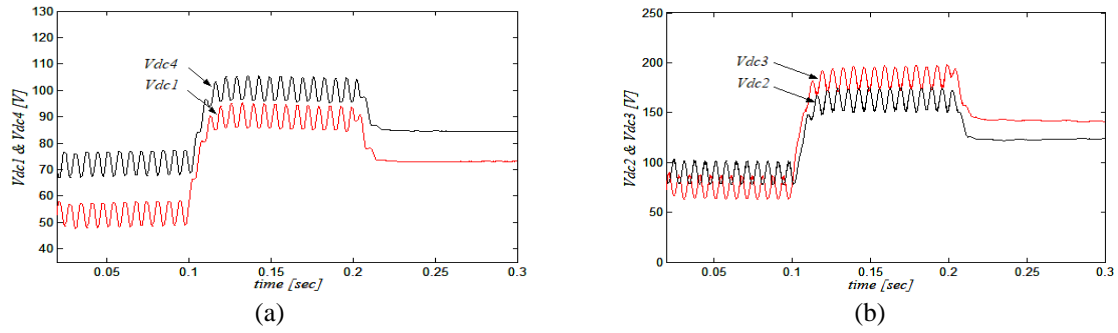Figure 9. Capacitor voltage at different levels with PI control, (a) V_{dc1} and V_{dc4} , (b) V_{dc2} and V_{dc3}

Figure 10. Capacitor voltage at different levels with SFC control, (a) V_{dc1} and V_{dc4} , (b) V_{dc2} and V_{dc3}
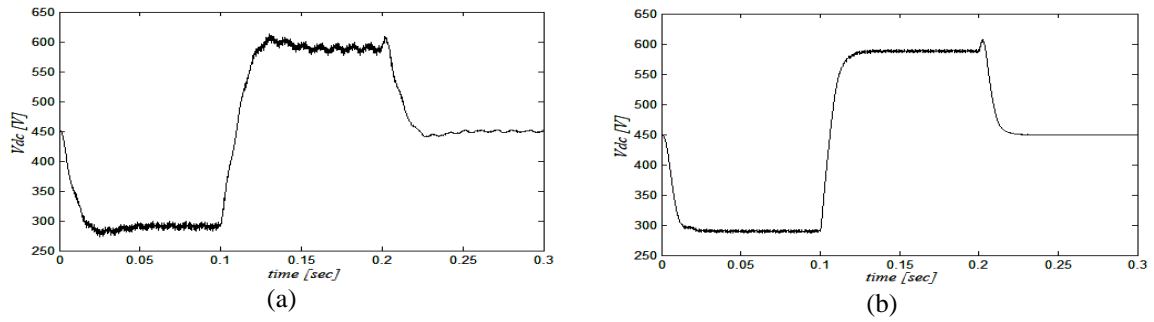

Figure 11. Total DC side voltage V_{dc} of the Inverter, (a) with PI control, (b) with SFC control
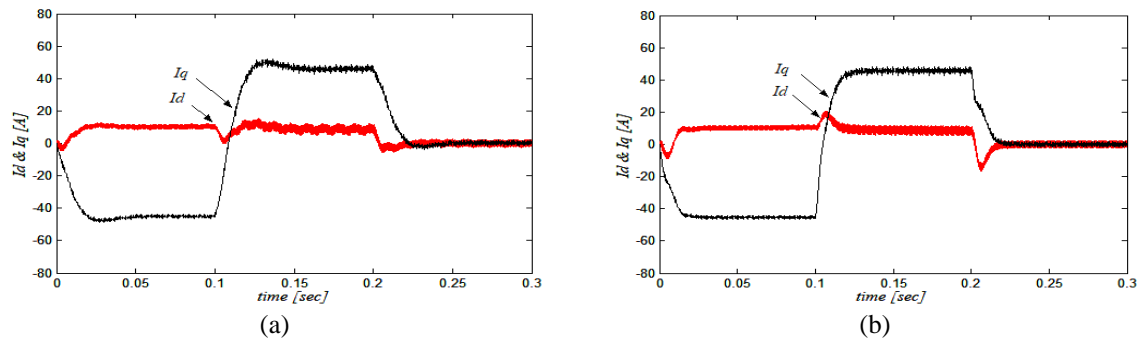

Figure 12. AC current in d-q frame, (a) with PI control, (b) with SFC control
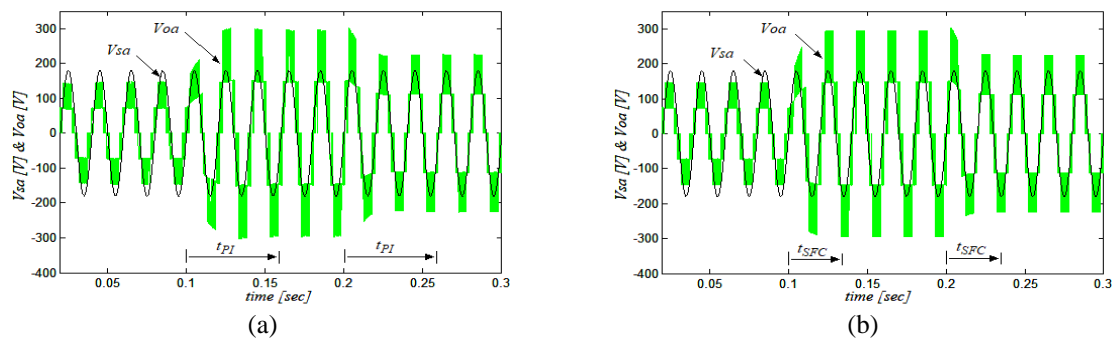

Figure 13. Inverter output voltage and source voltage, (a) with PI control, (b) with SFC control

5. CONCLUSION

In this paper, a simulation study of the dynamic performance and robustness of state feedback control have been proposed, evaluated and compared to a conventional PI controller applied to an ASVC compensator using five-level NPC-VSC inverter. The five-level NPC inverter has been used for its high quality waveshaping outputs.

Simulation results show the effectiveness of the proposed control strategy. The SFC control algorithm shows that reactive power compensation is achieved by controlling the exchange of active power between DC side of inverter circuit and AC system. It can be concluded that the SFC controller leads to improve transient response and hence provide fast reactive power compensation with balancing the total DC capacitors voltage. Also the SFC controller is better than the PI controller and can be easily tuned.

APPENDIX
SIMULATION PARAMETERS

$R_s = 1\Omega$, $L_s = 5\times10^{-3}$H, $C_s = 500\times10^{-6}$F, $V_s = 220$V, $m = 0.646$, $\omega = 100\pi$ [rad/sec], $K_p = 4.156\times10^{-6}$, $K_i = 2.4\times10^{-3}$, $m_f = 24$, $m_a = 0.8$, $A_c = 0.5$, $A_s = 0.8$, $f_c = 1200$Hz, $f_s = 50$Hz.

REFERENCES

[1] J. Fang, X. Li, H. Li and Y. Tang, "Stability improvement for three-phase grid-connected converters through impedance reshaping in quadrature-axis", *IEEE Transactions on Power Electronics,* vol. 33, no. 10, pp. 8365-8375, Oct. 2018.
[2] S. Yang, J. Fang, Y. Tang, H. Qiu, C. Dong and P. Wang, "Modular multilevel converter synthetic inertia-based frequency support for medium-voltage microgrids", *IEEE Transactions on Power Electronics,* vol. 66, no. 11, pp. 8992-9002, Nov. 2019.
[3] P.A. Blasco, R. Montoya-Mira, J. M. Diez, R. Montoya and M. J. Reig, "Compensation of reactive power and unbalanced power in three-phase three-wire systems connected to an infinite power network", *Applied sciences journal*, vol. 10, no. 1, p. 113, 2019.
[4] A. Gheewala, J. Chanawala, N. Jadav, M. Rishit, C. Machhi and J. Rana, "Load balancing and harmonic elimination using distribution static synchronous compensator (DSTATCOM)", *International Journal of Engineering and Techniques*, vol. 2, no. 2, pp. 184-190, Mar.- Apr. 2016.
[5] C. Dinakaran, "Implementation of Shunt and Series FACTS Devices for Overhead Transmission Lines", *International Electrical Engineering Journal (IEEJ) 2015*, vol. 6, no. 8, pp. 2009-2017, 2015.
[6] L. Kunjumuhammed, S. Kuenzel, B. Pal, "Modelling of flexible AC transmission system devices", *Simulation of Power System with Renewables, Academic press, ScienceDirect,* Chapter 8, pp. 205-224, Book 2020.
[7] S. Ali Al-Mawsawi, "Comparative analysis for optimum position of A PWM based UPFC and ASVC applied to multi-machine systems with non-linear load model," *International Journal of Advanced and Applied Sciences (IJAAS)*, vol. 6, no. 2, pp. 12-16, 2019.
[8] Y. Lee and H. Song, "A Reactive power compensation strategy for voltage stability challenges in the Korean power system with dynamic loads," *Sustainability*, vol. 11, no. 2, p. 326, Jan. 2019.
[9] S. Abazari and M. S. Payam, "Design of an optimized intelligent controller based on Lyapunov energy function for improving transient stability using the parallel FACTS devices", *Caspian Journal of Applied Sciences Research*, vol. 4, no. 1, pp. 1-111, Jan. 2015.
[10] K. Wang, M. Ye, W. Xiong, F. Wang and J. Hou, "Coordinated control of STATCOM and mechanically switched capacitors to improve short-term voltage stability," *2016 IEEE, In Proceedings of the POWERCON Conference*, Wollongong, Australia, 28 Sep.-01Oct. 2016.
[11] I. Muzaffer and M. ud din Mufti, "Modeling of a multi-machine system aided with power system stabilizers and shunt compensator for transient stability enhancement", *2017 IEEE, International Conference on Energy, Communication, Data Analytics and Soft Computing ICECDS 2017*, Chennai, India, 1-2 Aug. 2017.
[12] A. Nabae and I. Takahashi, "A new neutral point clamped PWM inverter," *IEEE Transactions on Industry Applications,* vol. 17, no. 5, pp. 509-517, Sep. 1981.
[13] A. Mandali, L. Dong and A. Morinec, "Advanced supplemental controller for a static var compensator in power systems", *2019 North American Power Symposium NAPS,* Wichita, KS, USA, 13-15 Oct. 2019.
[14] S. Shi, X. Wang, S. Zheng and F. Xia, "A New Diode-Clamped Multilevel Inverter for Capacitor Voltage Balancing", *Progress in Electromagnetics Research M*, vol. 52, pp. 181-190, 2016.
[15] VNSR. Murthy and A. Pandian, "Analysis of capacitor voltage balance in multilevel inverter," *International Journal of Applied Engineering Research*, vol. 12, no. 1, pp. 399-406, 2017.
[16] C. Gao, X. Jiang, Y. Li, Z. Chen and J. Liu, "DC-link voltage self-balance method for a diodeclamped modular multilevel converter with minimum number of voltage sensors," *IEEE Transactions on Power Electronics*, vol. 28, no. 5, pp. 2125–2139, May 2013.
[17] A. Ajami, H. Shokri and A. Mokhberdoran, "Parallel switch-based chopper circuit for DC capacitor voltage balancing in diode-clamped multilevel inverter", *IET Power Electronics*, vol. 7, no. 3, pp. 503-514, Mar. 2014.

[18] Mansour Benyamina, B. Mazari, A. Tahri, "A comparative study of robust control for an ASVC-based var flow compensation", *International Review of Electrical Engineering (IREE),* vol. 2 no. 5, pp. 681-686, Sep. 2007.

[19] A. Renault, M. Ayala, L. Comparatore, J. Pacher and R. Gregor, "Comparative study of predictive-fixed switching techniques for a cascaded H-bridge two level STATCOM", *2018 53rd International Universities Power Engineering Conference UPEC 2018*, Glasgow, UK, 4-7 Sep. 2018.

[20] L. Comparatore, A. Renault, J. Pacher, J. Rodas and R. Gregor, "Finite control set model predictive control strategies for a three-phase seven-level cascade H-bridge DSTATCOM", *2018 7th International Conference on Renewable Energy Research and Applications ICRERA 2018*, Paris, France, 14-17 Oct. 2018.

[21] K. A. Bhatt, B. R. Bhalja and U. Parikh, "*Controlled* switching technique for minimization of switching surge during energization of uncompensated and *shunt compensated* transmission lines for circuit breakers having pre-insertion resistors", *International Journal of Electrical Power & Energy Systems*, vol. 103, pp. 347-359, Dec. 2018.

[22] S. Babaei and S. Bhattacharya, "A control structure for PWM-controlled static synchronous compensators under unbalanced conditions and grid faults", *Science Direct, International Journal of Electrical Power & Energy Systems*, vol. 71, pp. 160-173, Oct. 2015.

[23] S. Ahmed, A. Gouichiche, E. Berkouk, "Optimized Total Harmonic Distortion PWM in Five Level Inverter with Differential evolution approach", *8th International Conference on Systems and Control ICSC 2019*, Marrakesh, Morocco, 23-25 Oct. 2019.

[24] E. Irmak, R. Bayindir and A. Köse, "Design and experimental analysis of an advanced static VAR compensator with computer aided control", *Science Direct, ISA Transactions*, vol. 64, pp. 384-393, Sep. 2016.

[25] C.R. Balamurugan, "A review on modulation strategies of multi level inverter", *Indonesian Journal of Electrical Engineering and Computer Science (IJEECS),* vol. 3 no. 3, pp. 681-705, Sep. 2016.

[26] O. Mäki, J. Turunen, J. Seppänen, K. Zenger and L. Haarla, "Robustness and performance of a multi-objective model predictive static var compensator controller", *Power Systems Computation Conference 2016, PSCC 2016,* Genoa, Italy, 2016.

[27] C.O. Omeje, "Mathematical modeling and stability analysis of a hybrid five-level static var compensation for efficient power transmission", *International Journal of Engineering Trends and Technology (IJETT)*, vol. 63 no. 1, pp. 17-27 Sep. 2018.

[28] K. Skandarama, R. C. Mala and N. Prabhu, "Control of bifurcation in a VSC based STATCOM", *Journal of Procedia Technology, elsevier*, vol. 21, pp. 187-195, 2015.

[29] B. Ch, U. R. Muduli and R. K. Behera, "Performance comparison of five-phase three-level NPC to five-phase two-level voltage source inverter", *2018 IEEE, International Conference on Power Electronics, Drives and Energy Systems PEDES 2018,* Chennai, India,18-21 Dec. 2018.

[30] Mansour Benyamina and B. Mazari, "Robust control techniques of ASVC-based var flow compensation", *Progress in Sustainable Energy Technologies*, *Springer*, vol. 2, pp. 489-502, Sep. 2014.

[31] M. Morari and E. Zafiriou, "Robust Process Control", Prentice Hall, Englewood Cliffs, NJ, 1989.

[32] Y. Feng, H. Zhao, M. Zhao and H. Chen, "A feedback linearization control scheme based on direct torque control for permanent magnet synchronous motor", *IEEE 2018, 37th Chinese Control Conference CCC 2018*, Wuhan, China, 25-27 Jul. 2018.